Cell Reports, Volume *23*

Supplemental Information

Intrinsic Instability of BOK

Enables Membrane Permeabilization in Apoptosis

Janet H. Zheng, Christy R. Grace, Cristina D. Guibao, Dan E. McNamara, Fabien Llambi, Yue-Ming Wang, Taosheng Chen, and Tudor Moldoveanu

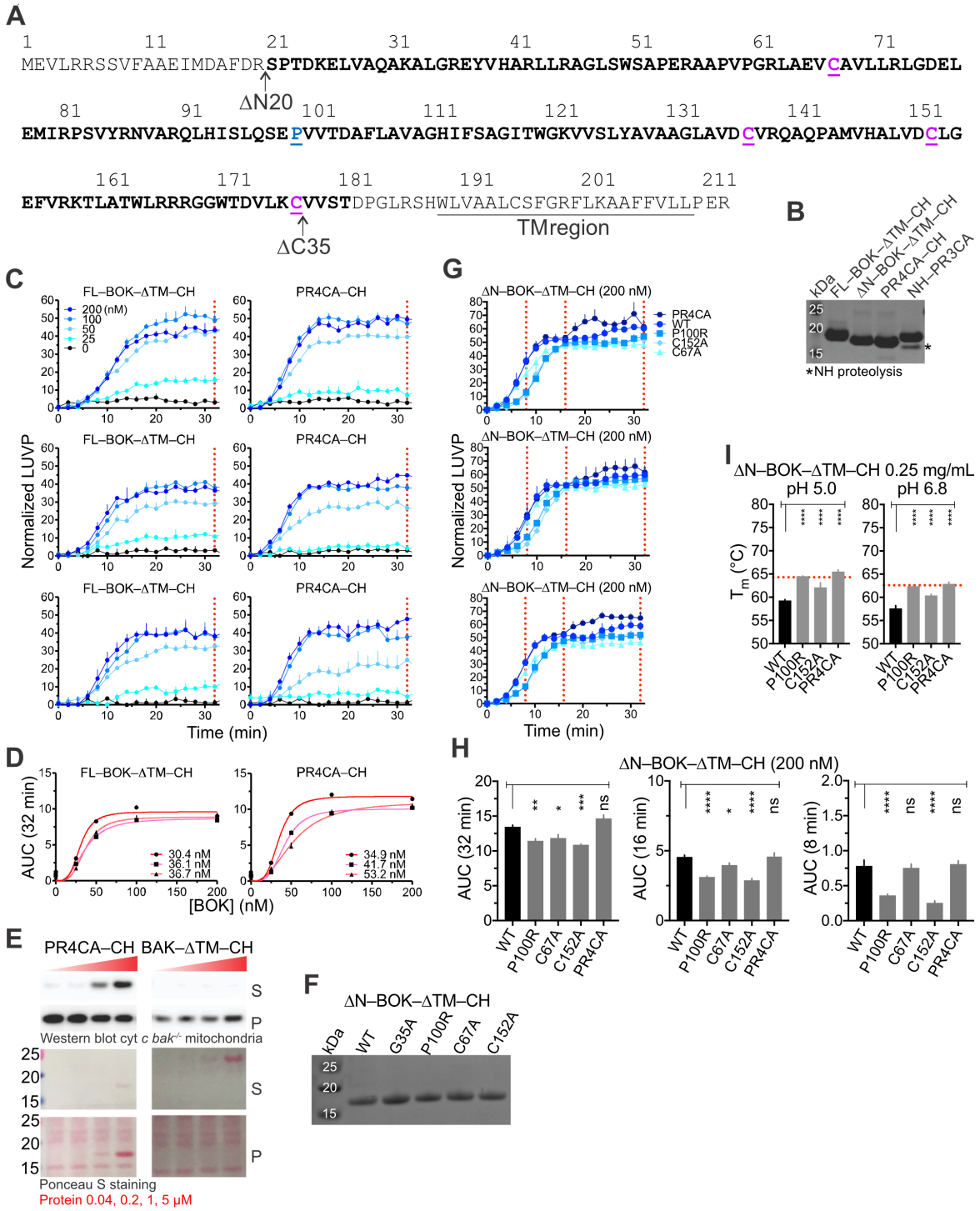

Figure S1. Related to Figure 1 | BOK engineering, LUVP, MOMP and TSA analyses.

(A) Summary of human BOK engineering described in Figure 1A is illustrated on the primary sequence.

(B) SDS–PAGE analysis of purified BOK constructs and their mutants. FL, full length; NH, N-terminal His tag; CH, C-terminal His tag; PR4CA and PR3CA are combined mutants C67A, P100R, C137A, C154A, with and without C177A, respectively; PR4CA–CH and NH–PR3CA

are the corresponding mutants in ΔN–BOK–ΔTM–CH and NH–ΔN–BOK–ΔTM, respectively.

(C) Normalized LUVP data for the BOK constructs described in Figures 1B and 1C represent the average and (standard deviation) SD for 3 independent experiments performed in triplicate.

(D) AUC at 32 min plotted as a function of protein concentration for the BOK constructs described in panel c was fitted to the Hill equation. BOK concentration required to achieve half-maximal AUC values for the 3 experiments are indicated. These values were averaged to generate the data given in Figure 1D.

(E) Independent replicate of the MOMP assay presented in Figure 1E.

(F) SDS–PAGE analysis of purified WT and point mutant ΔN–BOK–ΔTM–CH proteins used in panels g-i. The G35A mutant will be described in detail later.

(G) Normalized LUVP data for the WT and ΔN–BOK–ΔTM–CH mutants described in panel f represent the average and SD for 3 independent experiments performed in triplicate at 200 nM concentration.

(H) Combined average and standard error (SE) AUC at 32, 16, and 8 min for the LUVP induced by WT and ΔN–BOK–ΔTM–CH mutants in panel G.

(I) Representative replicate of thermal denaturation measured by TSA at 0.25 mg/mL for WT and ΔN–BOK–ΔTM–CH mutants. Data represent average thermal melting (T_m) and SD of quadruplicate measurements. The red dotted line represents 5 °C above the average WT T_m.

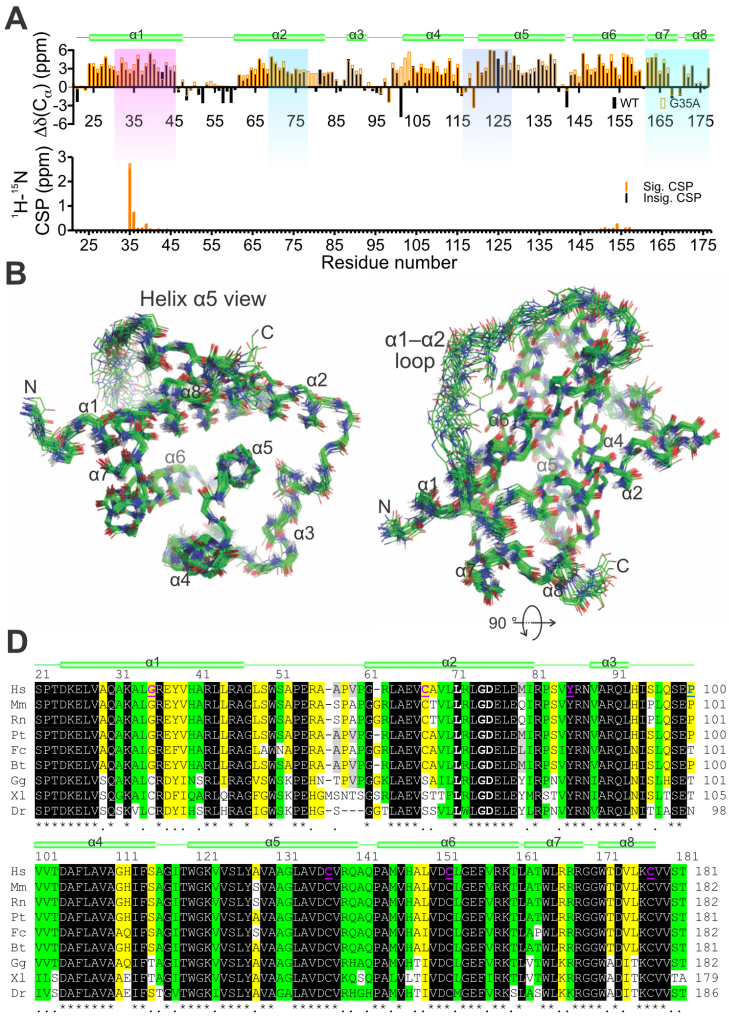

C

NMR distance and dihedral constraints	BOK
Distance constraints	
Total number of NOEs	1832
Intramolecular	595
Short range (|i-j| ≤ 1)	506
Medium-range (1 ≤ |i-j| ≤ 5)	330
Long-range (|i-j| ≥ 5)	401
Hydrogen bonds	190
Total dihedral angle constraints	
Phi (ϕ)	118
Psi (ψ)	118
Target function	1.33 ± 0.25
Violations	
Upper Distance (max) (Å)	0.34 ± 0.09
Lower Distance (max) (Å)	0.14 ± 0.08
Angle (max) (°)	3.76 ± 1.43
Average pairwise r.m.s. deviation (Å)[a]	
Backbone	0.64 ± 0.11
Heavy atom	1.08 ± 0.09
Ramachandran statistics	
Residues in most favorable region	83.3 %
Residues in additional favorable region	11.5 %
Residues in generously allowed region	4.6 %
Residues in disallowed region	0.5 %

Figure S2. Related to Figure 2 | NMR analysis of the BCL-2 core of BOK.

(A) Plot of C_α chemical shift deviation from random coil as a function of residue number for WT and G35A PR3CA (top). Chemical shift perturbation (CSP) analysis between backbone amides of WT and G35A localize nearby G35A (bottom).

(B) Backbone heavy atoms representation of the top 20 lowest-energy NMR structures.

(C) NMR structure calculation and refinement statistics for PR3CA ΔN20–BOK–ΔC35.

(D) Sequence alignment of the BCL-2 core of BOK from *Homo sapiens* (Hs), *Mus musculus* (Mm), *Rattus norvegicus* (Rn), *Pan troglodytes* (Pt), *Felis catus* (Fc), *Bos taurus* (Bt), *Gallus gallus* (Gg), *Xenopus laevis* (Xl), and *Danio rerio* (Dr). The amino acid residues mutated in this study are underlined and color-coded on the Hs sequence. Sequence identity is highlighted as follows: black (100%), green (<75%), yellow (<50%), and grey (<33%).

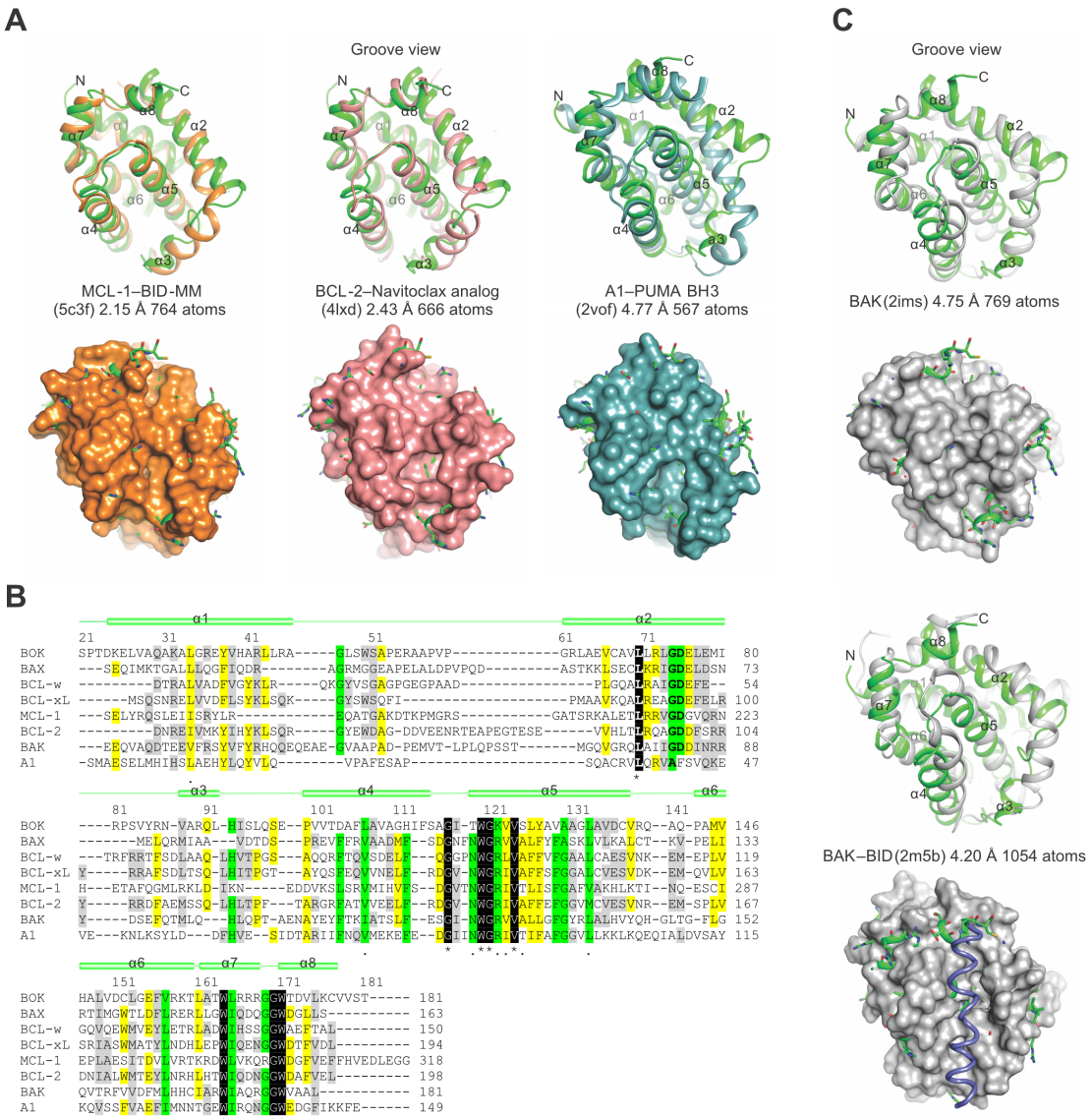

Figure S3. Related to Figure 3 | Structure and sequence alignment of BOK with BCL-2 proteins reveals an atypical hydrophobic groove.

(A) Structure alignment of the BCL-2 core of BOK (green) and that of MCL-1, BCL-2, and A1 done in Pymol. The root-mean-square deviation is indicated for the total number of atoms used in the alignment. In the top panels, the cartoon representations indicate major deviations in alignments in the region connecting helices α2–α4, which defines the atypical groove of BOK. Bottom panels show the cartoon-and-stick representations of BOK protruding through the surface representation of the aligning partner. Clashes with incoming hydrophobic ligands are predicted throughout the hydrophobic groove of BOK.

(B) Sequence alignment of the BCL-2 family proteins was done on the basis of the structure alignment in Figure 3A and panels S3A and S3C. Sequence identity is highlighted as follows: black (100%), green (<75%), yellow (<50%), and grey (<33%).

(C) Structure alignment of the BCL-2 core of BOK (green) and that of apo-BAK (grey) and the BID SAHB–BAK complex (grey and blue) was done as in panel A.

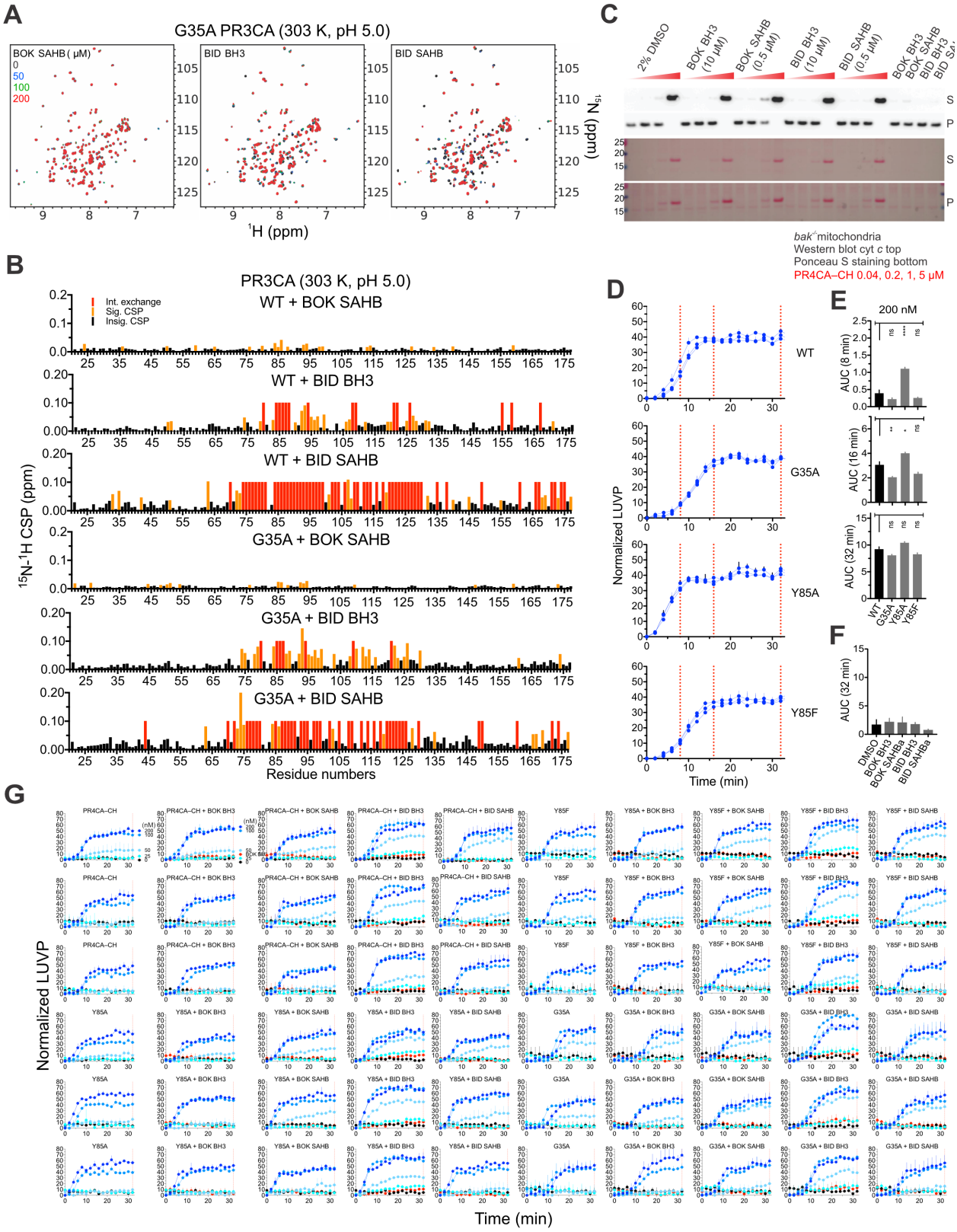

Figure S4. Related to Figure 4 | NMR titrations of BOK and BH3 peptides and LUVP analysis reveal binding-induced activation in liposome permeabilization.

(A) $^{1}H–^{15}N$ TROSY spectra of ^{15}N-labeled G35A PR3CA titration with BOK SAHB, BID BH3, and BID SAHB at pH 5.0. All peptides were titrated at the same concentrations indicated for BOK SAHB.

(B) CSP analysis of WT and G35A PR3CA with 200 μM peptide at 303 K and pH 5.0. Intermediate (int.) exchange residues have been assigned 0.1 ppm. Significant (sig.) and insignificant (insig.) CSPs were calculated as previously described (Schumann et al., 2007).

(C) Independent replicate of the MOMP assays presented in Figure 4D.

(D) Average and SD of LUVP for three independent experiments performed in triplicate for WT and mutant PR4CA–CH at 200 nM.

(E) Combined average and SE of AUC at 8, 16, and 32 min for the LUVP analysis in panel D.

(F) Combined average and SD of AUC at 32 min for the normalized LUVP of BH3 peptides in panel G.

(G) Normalized LUVP for WT, G35A, Y85A, and Y85F PR4CA–CH in the presence of unstapled and stapled BH3 peptides and DMSO vehicle control. Peptide concentrations were empirically selected to induce low or no LUVP in the absence of BOK and were 10 μM BOK and BID BH3, 0.13 μM BOK SAHB, 0.5 μM BID SAHB. Data represent average and SD of three experiments done in triplicate.

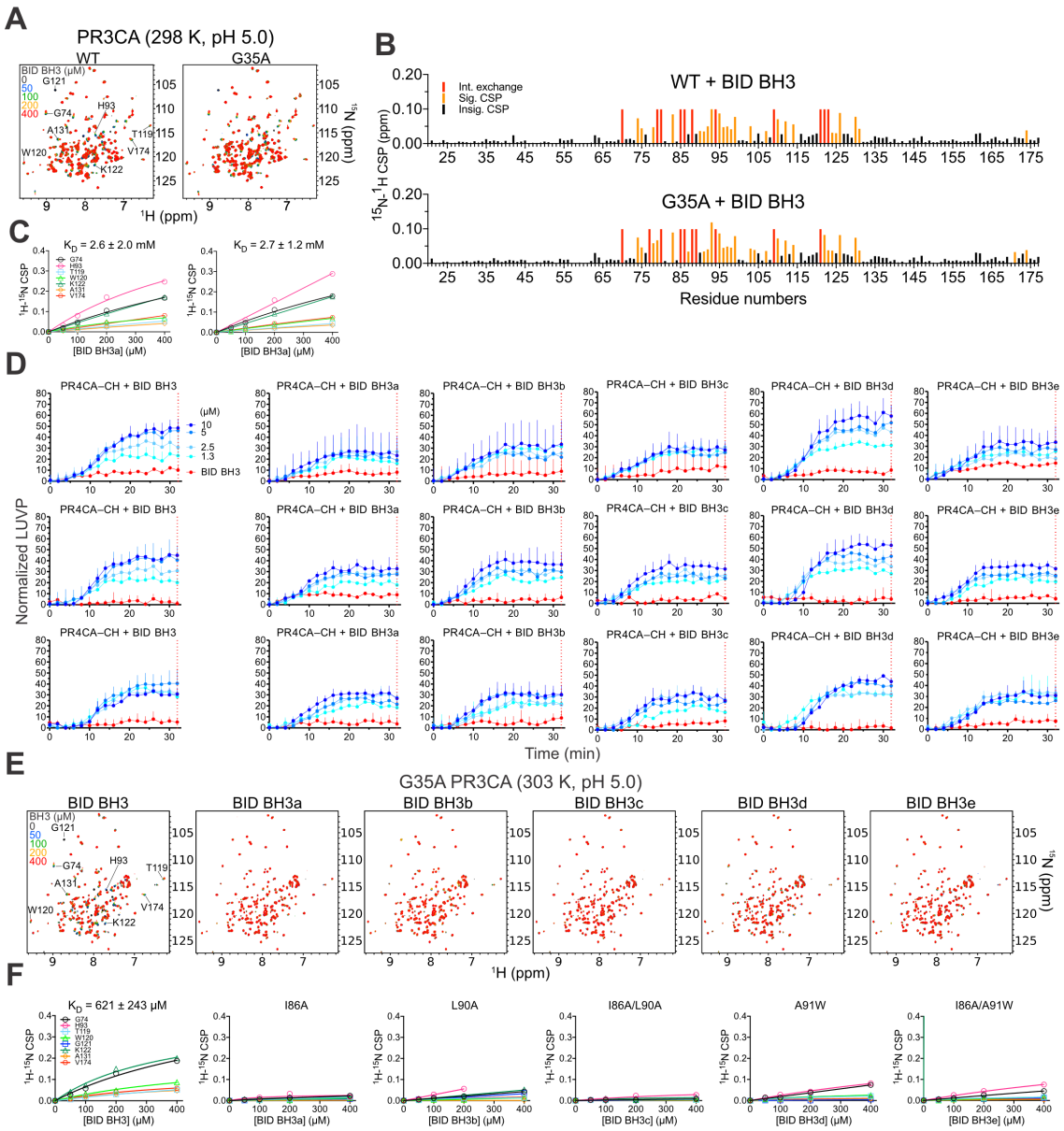

Figure S5. Related to Figure 5 | BID BH3 binding to the canonical groove of BOK is pH dependent.

(A) Overlay of ^{1}H–^{15}N TROSY spectra of ^{15}N-labeled WT and G35A PR3CA titration with WT and mutant BID BH3 at 298 K and pH 5.0.

(B) CSP analysis of WT and G35A PR3CA at 400 μM peptide from panel a. Intermediate (int.) exchange residues have been assigned 0.1 ppm. Significant (sig.) and insignificant (insig.) CSPs were calculated as previously described (Schumann et al., 2007).

(C) CSPs plotted against concentration for indicated residues were fitted to a hyperbola to determine the K_D for the interactions in panel A.

(D) Normalized LUVP for WT PR4CA–CH in the presence of unstapled WT and mutant BID BH3 peptides. Peptide concentrations were empirically selected to induce low or no LUVP in the

absence of BOK.

(E) Overlay of $^{1}H–^{15}N$ TROSY spectra of ^{15}N-labeled G35A PR3CA titration with WT and mutant BID BH3 at 303 K and pH 5.0.

(F) CSPs plotted against concentration for indicated residues were fitted to a hyperbola to determine the K_D for the interaction of G35A PR3CA and WT BID BH3 peptide. Mutant BID BH3 peptides exhibited weaker binding to BOK compared to the WT.

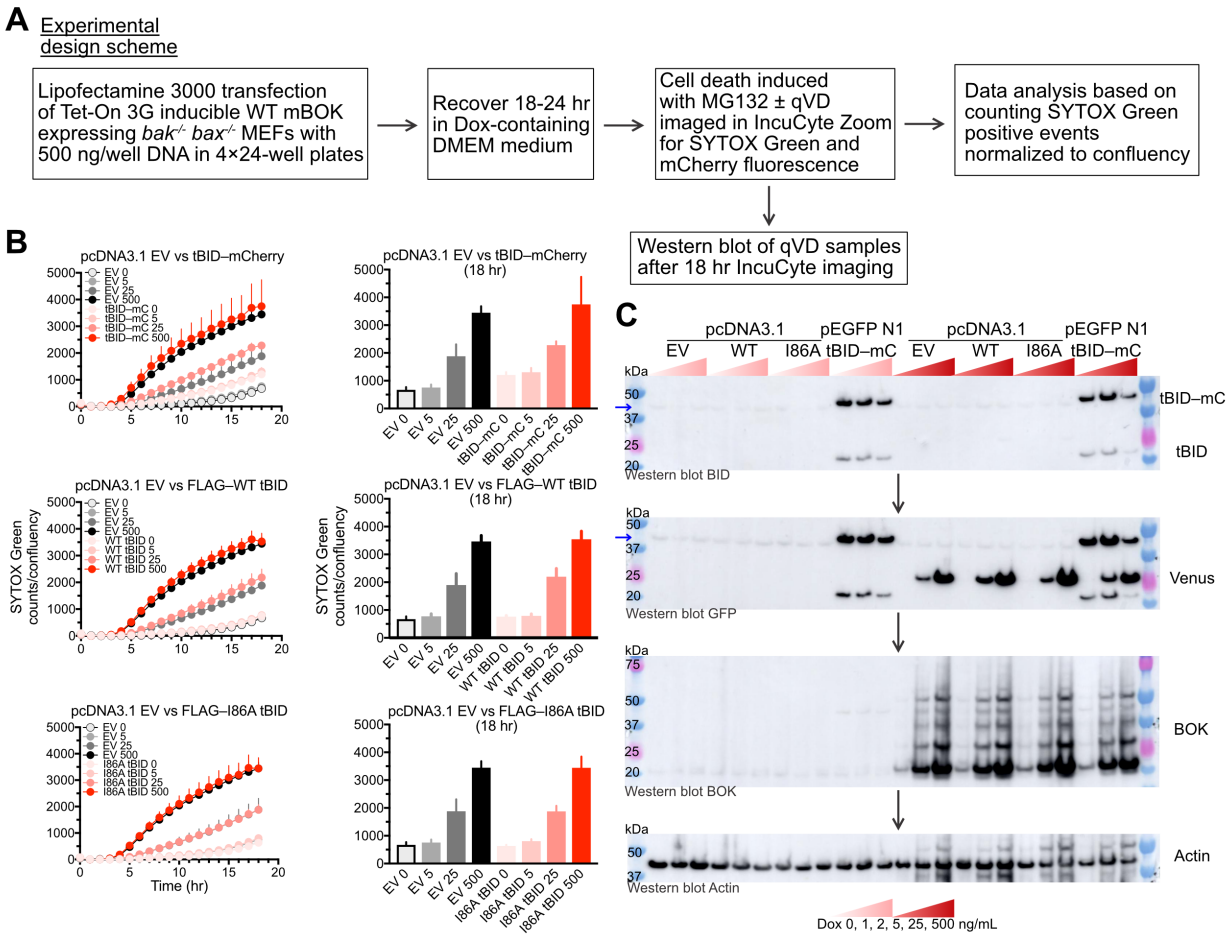

Figure S6. Related to Figure 6 | Transient transfection of tBID does not trigger BOK-mediated cell death.

(A) Schematic of the transient transfection protocol.

(B) Cell death induced by WT (mouse) mBOK is insignificantly affected by transient transfection of pcDNA3.1 empty vector (EV), FLAG–WT tBID, FLAG–I86A tBID, or tBID–mCherry (tBID–mC). The *bak*$^{-/-}$ *bax*$^{-/-}$ MEFs do not express detectable levels of endogenous BID, and show clear expression of tBID–mCherry but not the FLAG–tBID, which may be attributed to the difference in promoter strength between the modified pEGFP N1 vector and pcDNA3.1. Cell death was monitored hourly by IncuCyte imaging of SYTOX Green staining. The 18 hr time point indicate insignificant differences between the empty vector and tBID–mCherry samples at each Dox concentration. BOK protein was not detected below 5 ng/mL Dox. Banding pattern indicates potential BOK ubiquitination. Data represent average and SD of triplicate.

(C) Transient transfection of vectors expressing FLAG–tBID and tBID–mCherry (tBID–mC) was performed according to the scheme in panel A. After recovery in the respective doses of Dox, cell death was induced with MG132 for 18 hr. Western blotting of samples treated with the caspase inhibitor qVD was done sequentially with BID, GFP, BOK, and Actin antibodies. The blue arrows in the BID and GFP blots indicate cross reactivity by the BID antibody with a band that migrates slightly faster than tBID–mCherry. Weak production of tBID alone is also detected,

perhaps being generated through proteolysis of tBID–mCherry.

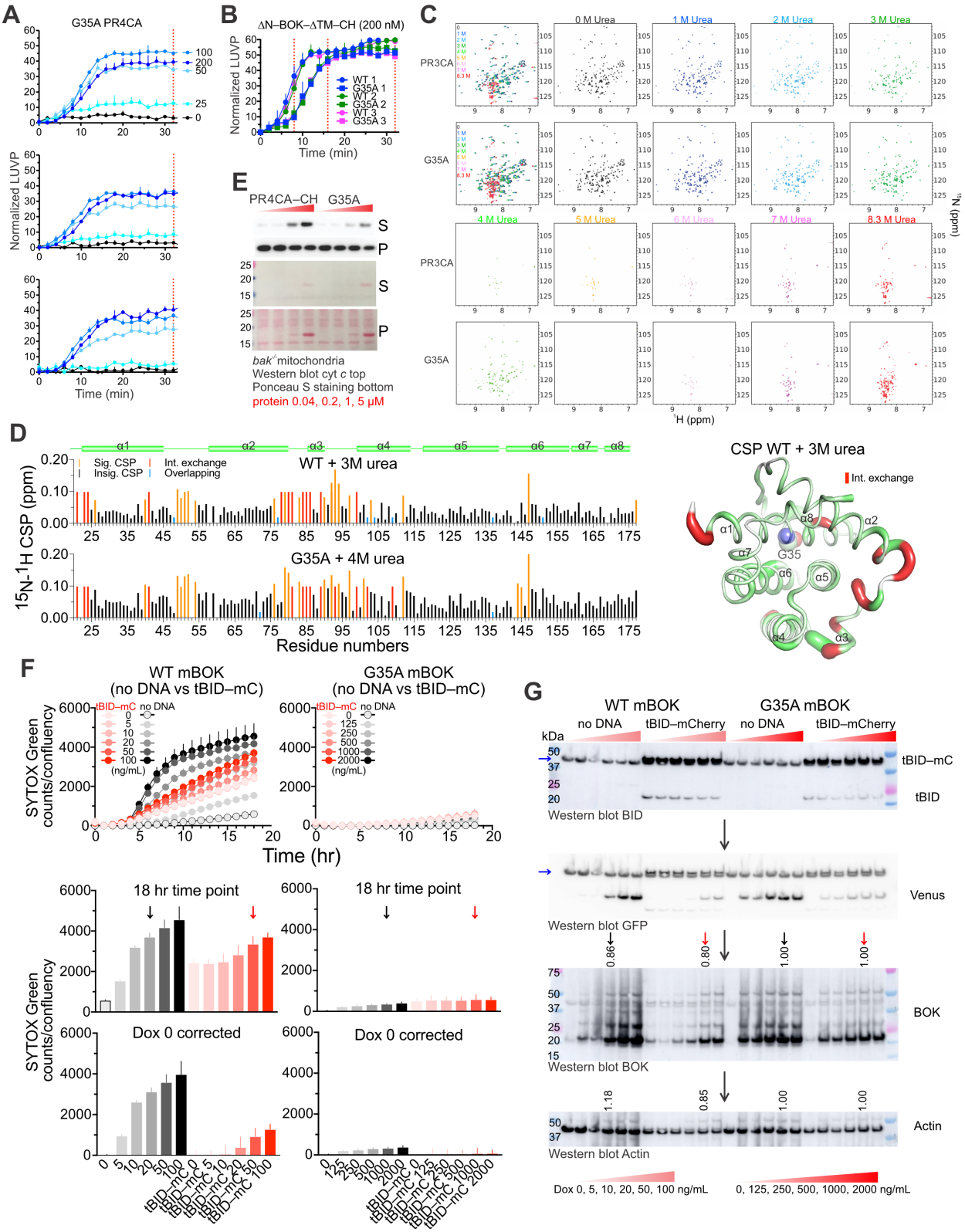

Figure S7. Related to Figure 7 | Intrinsic instability in helix α1 facilitates membrane

permeabilization to promote cell death.

(A) Normalized LUVP data for G35A PR4CA–CH mutant described in Figure 7A was performed side-by-side with the samples presented in Figure S1C and represent the average and SD for 3 independent experiments performed in triplicate.

(B) Normalized LUVP data for WT and G35A ΔN–BOK–ΔTM–CH described in Figure 7A represent the average and SD for 3 independent experiments performed in triplicate.

(C) $^{1}H–^{15}N$ TROSY spectra of ^{15}N-labeled WT and G35A PR3CA titration with urea indicate unfolding transition at higher urea concentration for the stabilizing mutant G35A compared to WT.

(D) CSP analysis of the data in panel c indicates similar binding by urea of WT and G35A PR3CA BOK. Urea interacting regions are largely confined to the N-terminal bundle, including the N- and C-termini of helix α1, loop between helices α1 and α2, and the region spanning the C-terminus of helix α2 and N-terminus of α4. Importantly, helix α1 does not exhibit differences between WT and G35A, suggesting that its unfolding during membrane association is potentially regulated. Putty thickness correlates with CSP magnitude.

(E) Independent replicate of the MOMP assay presented in Figure 7D.

(F) Transient transfection with tBID–mCherry (tBID–mC) of WT and G35A mBOK expressing cells was performed according to the scheme in Figure S6a. The mock control was performed by incubating cells similar to the tBID–mCherry transient transfection but in the absence of DNA and transfection reagents (no DNA). After recovery in the respective doses of Dox, cell death was induced with MG132 for 18 hr. Cell death induced by WT and G35A mBOK was monitored hourly by IncuCyte imaging of SYTOX Green staining. The 18 hr time points indicate significant differences between the tBID–mCherry WT and G35A samples at all Dox concentration. The mock control shows that transient transfection of tBID–mCherry was toxic as indicated by significant cell death in the absence of Dox (Dox 0). Black and red arrows show comparable levels of BOK as determined in panel G. Data represent average and SD of triplicate measurements.

(G) Western blotting of samples treated with the caspase inhibitor qVD for the experiment in panel F was done sequentially with BID, GFP, BOK, and Actin antibodies. The blue arrows in the BID and GFP blots indicates cross reactivity by the BID antibody with a band that migrates slightly faster than tBID–mCherry. Weak production of tBID alone is also detected, perhaps being generated through proteolysis of tBID–mCherry. Banding pattern indicates potential BOK ubiquitination. Black and red arrows show comparable levels of BOK, which have been integrated and normalized to G35A. Their values are indicated below the arrows.